The Unprecedented Pacific Northwest Heatwave of June 2021

Rachel White (rwhite@eoas.ubc.ca)
University of British Columbia https://orcid.org/0000-0002-3650-3019

Sam Anderson
University of British Columbia https://orcid.org/0000-0001-6757-6846

James Booth
City College of New York; City University of New York - The Graduate Center

Ginni Braich
University of British Columbia

Christina Draeger
University of British Columbia

Cuiyi Fei
University of British Columbia

Christopher Harley
University of British Columbia https://orcid.org/0000-0003-4099-943X

Sarah Henderson
British Columbia Centre for Disease Control (BCCDC); University of British Columbia
https://orcid.org/0000-0002-3329-184X

Matthias Jakob
BGC Engineering Inc; University of British Columbia

Carie-Ann Lau
BGC Engineering Inc

Lualawi Mareshet Admasu
University of British Columbia

Veeshan Narinesingh
City University of New York – The Graduate Center

Christopher Rodell
University of British Columbia

Eliott Roocroft
University of British Columbia

Kate Weinberger
University of British Columbia

Greg West
BC Hydro; University of British Columbia

Physical Sciences - Article

Keywords:

Posted Date: April 26th, 2022

DOI: https://doi.org/10.21203/rs.3.rs-1520351/v1

The Unprecedented Pacific Northwest Heatwave of June 2021

Rachel H. White, Sam Anderson, James F. Booth, Ginni Braich, Christina Draeger, Cuiyi Fei, Christopher D. G. Harley, Sarah B. Henderson, Matthias Jakob, Carie-Ann Lau, Lualawi Mareshet Admasu, Veeshan Narinesingh, Christopher Rodell, Eliott Roocroft, Kate R. Weinberger, Greg West

In late June to early July 2021 a heatwave of unprecedented magnitude impacted the Pacific Northwest region, lands colonially named British Columbia (BC) and Alberta (AB) in Canada, and Washington (WA) and Oregon (OR) in the United States. Many locations broke all-time maximum daily temperature records by more than 5°C. The standing Canadian national temperature record was broken on three consecutive days, at multiple locations, with the highest temperature of 49.6°C recorded, 4.6°C higher than the previous Canadian record. Weather forecasts provided advanced notice of the severity of the event, while sub-seasonal forecasts showed substantially increased likelihood of atmospheric blocking and high temperatures with 10-day lead times, and some skill out to 18 days. The impacts of this event were catastrophic. Estimates indicate at least 900 attributable deaths occurred across BC, WA and OR, likely the deadliest weather event in Canadian[1] history. The heat contributed to mass-mortalities of marine life, reduced crop and fruit yields, river flooding from rapid snow and glacier melt, and a rapid increase in wildfires—the latter contributing to devastating landslides in the months following.

An unprecedented heatwave

The unprecedented Pacific Northwest heatwave occurred from approximately 25 June to 2 July 2021, during which near-surface air temperature anomalies were 16-20°C above normal (Fig. 1b) and many locations broke all-time maximum daily temperature records by more than 5°C (Fig. 1a). The standing Canadian national temperature record was broken three days in a row, at multiple locations, with the highest temperature of 49.6°C recorded in Lytton, BC, on 29 June (Fig. 1b), 4.6°C higher than the previous Canadian record temperature. Lytton, a small town in an arid mountain valley in the lee of the BC Coast Range, is located on Lytton First Nation reserves, at the site of the Indigenous village of Kumsheen on the traditional lands of the Nlaka'pamux people. The following day much of Lytton was tragically destroyed by a wildfire. The new record temperature was reportedly the hottest worldwide temperature recorded north of 45° latitude (Lytton is just north of 50°, and is shown by the small triangle in Fig. 1a), and hotter than any recorded temperature in Europe or South America [2]. The degree to which records were broken was extraordinary when compared with the infamous heatwaves in Europe in August 2003 and Russia in July-August 2010 (see Fig. 1 and Supplementary Fig. S1), both of which killed 10,000s of people [3,4]. Notably, whilst the magnitude was much higher, the June 2021 heatwave was shorter than these previous two heatwaves.

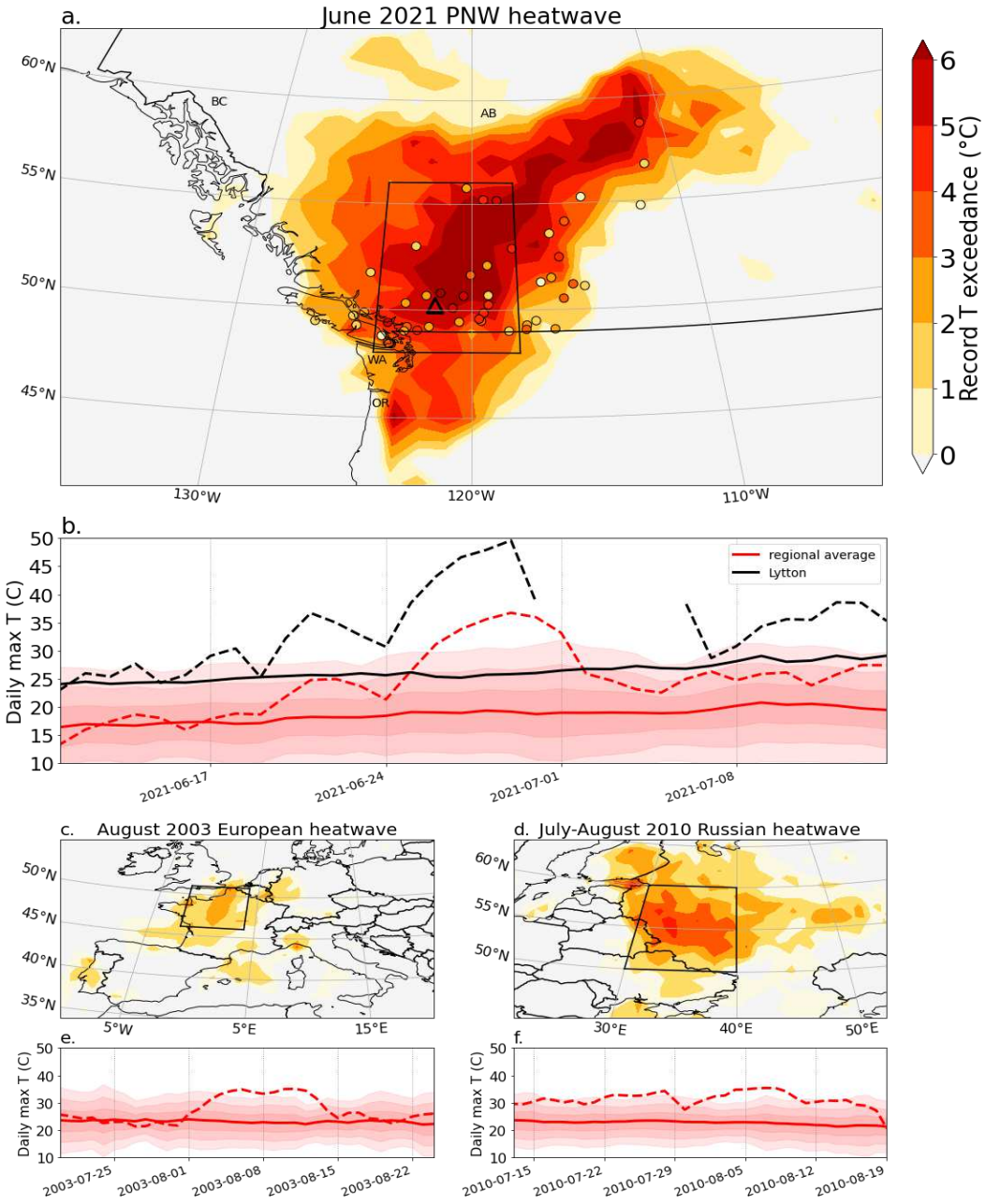

Figure 1. The June 2021 Pacific Northwest (PNW) heatwave (a and b) in contrast to the European heatwave of August 2003 (c and e) and the Russian heatwave of July-August 2010 (d and f). Panels (a), (c) and (d) show exceedance of the previous high temperature record in near-surface (2 m) air temperature during the heatwave period. Filled contours show ERA5 reanalysis data (all using the colour-scale in panel a.). Individual markers in panel (a) show observational station data in Canada; the triangle is Lytton, where the new Canadian high temperature record was set. Panels (b), (e) and (f) show the evolution of daily maximum temperature (red dashed) for the spatial average over the black box in the corresponding map and the 1980-2020 climatological mean (solid red), with shading +/-1, 2 and 3 standard deviations from these 40 years. In panel (b), the black lines show values from the Lytton, BC weather station (missing values from 1-5 July are likely due to the wildfire).

Synoptic conditions

The synoptic conditions leading to this event can be traced back about a week prior to onset on 25 June. From 19-21 June a low pressure system intensified southeast of the Kamchatka Peninsula of eastern Russia; the associated northerly winds transporting cold air southward over the northwest Pacific Ocean. Concurrently, a developing low pressure system west of Japan brought a warm, moist airmass northward into the same region. The juxtaposition of these two airmasses created a strong temperature gradient, supporting the formation of a strong (>75 ms^{-1} at the 200-hPa level) west-east oriented jet over the western Pacific. Another low pressure system developed west of Japan from 22-23 June. Southerly flow ahead of the low, and condensational heating within clouds, contributed to low-level warming. Such low-level warming is known to be associated with building high pressure ridges; ridging developed within the strong jet, initiating a wave that propagated eastward across the Pacific.

From 23-24 June the upper-level wave energy transiting the Pacific deepened the upper-level trough, and the surface low also intensified. The associated southerly flow brought warmer air into the eastern Pacific; combined with condensational heating within clouds, this built high pressure ridging over the eastern Pacific (Fig. 2a)—the high-amplitude ridge associated with the unprecedented heatwave. A final surface low formed over the east-central Pacific (near 150°W, 40°N) on 24 June and persisted into the 28th, again acting to further amplify the ridge (Fig. 2b). Quasi-stationary high pressure ridges such as this are known as a block or blocking high.

Near-surface temperature anomaly plots show dramatic warming from 24-27 June (Figs. 2c and d). Backwards air parcel trajectories reveal that the low-level airmass warmed because it 1) originated from a warmer source region closer to the equator, 2) underwent diabatic (presumably condensational) heating within low pressure systems over the eastern Pacific, and 3) underwent adiabatic warming as it subsided under strong high pressure ridging (see Methods, and Overland 2021[5]). Locally, the airmass underwent further diabatic (sensible) heating from the land surface under clear sky conditions (i.e, shortwave radiative forcing [6]); the heatwave occurred notably close to the summer solstice. Lytton, which recorded the heatwave's hottest temperature, lies within an arid, steep, rocky canyon, providing conditions for particularly intense sensible heating, with effects compounding over multiple days. A coastal thermal trough [7] enhanced the coastal pressure gradient, bringing so-called "outflow" winds from the interior to coastal population centers (e.g., Vancouver, Seattle, Portland). These contributed additional warming because 1) hotter air from the interior was transported to the coast, and 2) adiabatic warming occured as the air traveled from higher interior elevations towards the coast.

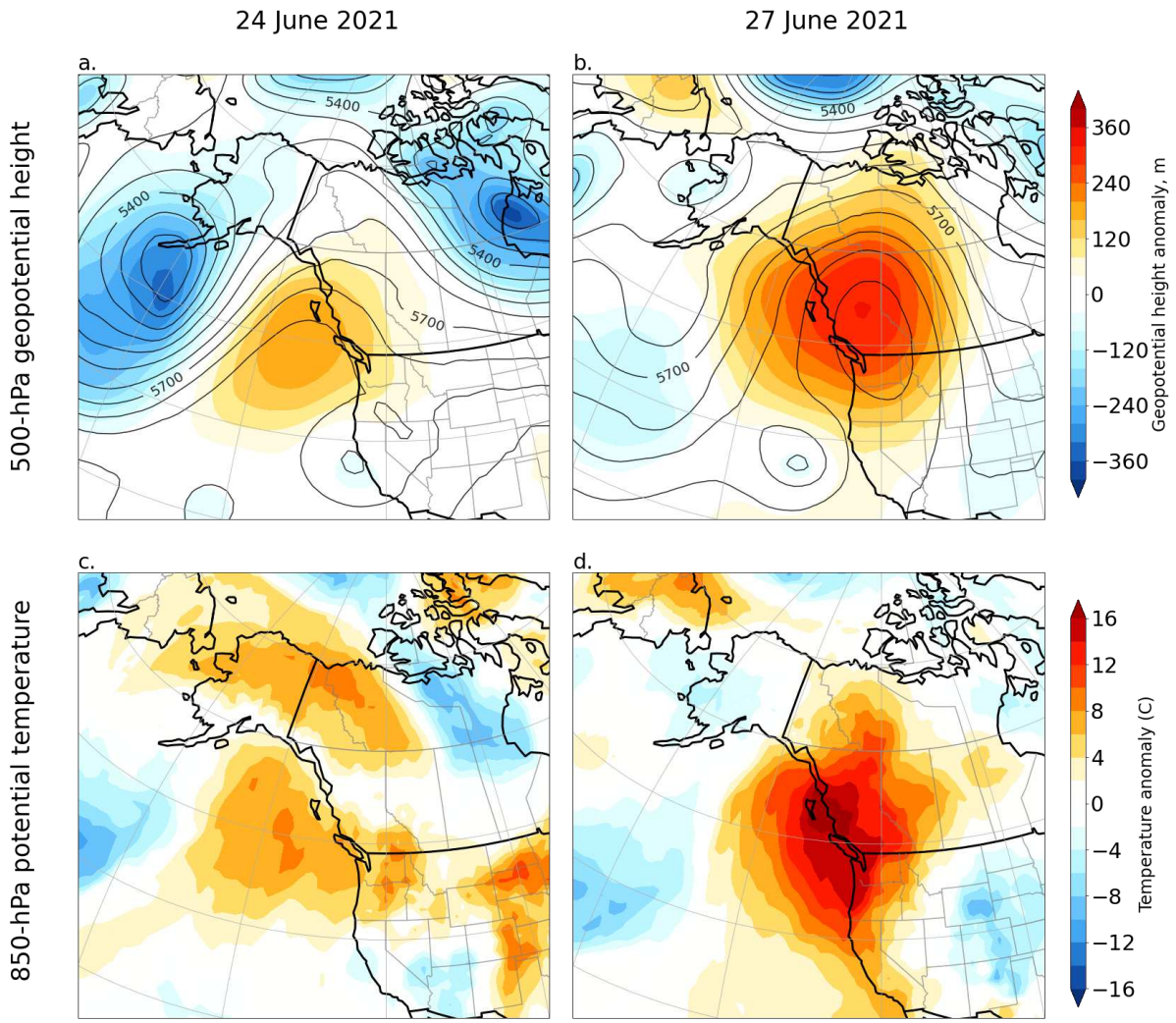

Figure 2. Upper panels (a and b) show upper-level (500-hPa) geopotential heights (contoured, m, contour interval 60 hPa) and anomalies from 1980-2020 climatology (shaded, m). Lower panels (c and d) show 850-hPa temperature anomalies (shaded, °C). Left panels are for 24 June, and right panels for 27 June.

Forecasts

We consider the evolution of forecasts for this event from a state-of-the-practice forecast system during the 8 days prior to the heatwave onset, and provide an operational meteorologist's perspective with respect to interpretation and communication of the forecasts. See Methods for a primer on ensemble forecasting and a description of the forecast system.

On 18 June, 8 days before the onset of the extreme heatwave and 12 days before it peaked, the ensemble forecast gave its first indication of a heatwave. At this point, meteorologists were more focused on a different heatwave earlier in the forecast period (21-22 June, see Fig. 1b). Given the known lower forecast skill at longer horizons, and the moderate heatwave forecast (resulting from the averaging of disparate scenarios provided by the ensemble members), meteorologists communicated that a second heatwave was *likely* for the following weekend.

By 21 June, 5 days before the onset and 9 days before it peaked, the forecast ensemble clearly indicated an extreme heatwave—daily records would likely be broken, and all-time records looked possible. For the typically hottest areas of the province in the Southwest Interior (including Lytton), the forecast indicated that temperatures in the mid-40's were possible. Meteorologists are typically reluctant to make extreme forecasts at 5- to 9-day forecast horizons for fear of "crying wolf" and the associated reduction in end-user trust. In this case, however, certainty from the ensemble forecast was high enough that meteorologists were able to warn of "extreme" heat at this relatively long lead time—a testament to ensemble forecast technology.

From 23-25 June, the forecasted "most likely" temperatures continued to increase, as well as the longevity of the heatwave, particularly for interior BC. Meteorologists were able to communicate certainty about all-time records being broken, and warn about potential impacts. By the onset of the heatwave on 25 June (4 days before it peaked), forecasts of the magnitude and longevity of the event were very good; although forecasted high temperature records fell 1-3°C short of the observed highs in many cases.

Subseasonal forecasts

The ability to forecast extreme events at longer lead times can significantly enhance early warning and preparation systems. Sub-seasonal to seasonal (S2S) forecasts fill the gap between the short to medium range weather forecasts discussed in the previous section, and seasonal forecasts (3 months lead time and beyond). We analyse the prediction of this heatwave event using the European Centre for Medium-Range Weather Forecasts (ECMWF) operational S2S forecasts. We look for prediction of temperatures or frequency of blocking above the 95th percentile (referred to as 'extreme' in the following text), as no ensemble members of any S2S forecasts predicted temperatures as extreme as those observed for intializations earlier than 17 June [8].

Figure 3 shows an increased probability of extreme temperatures across 25 June-1 July in forecasts initialized from 10 June onwards, consistent with Lin et al. (2022)[8]. From 14 June, up to 70% of ensemble members forecasted extreme temperatures somewhere within the affected region, with the predicted location improving with shorter lead times, consistent with the weather forecast analysis described above. An increased probability of extreme blocking is seen in forecasts at lead times as early as 7 June—up to 3 times the climatological frequency. This is not associated with an increased probability of extreme temperatures over the affected region, however, likely due to errors in forecasted block location placing the block too far west over the ocean. For forecasts initialized on 7 and 10 June, a higher probability of extreme temperature anomalies is predicted to the east of the heatwave region, consistent with a widespread soil moisture deficit across this region at the time (not shown).

Interestingly, a stronger forecast in terms of both temperature and blocking frequency is seen for forecasts initialized on 14 June when compared to forecasts initialized on 17 June (Figs. 3d-e and i-j). The *location* of the extreme temperature anomalies and blocking did, however, improve with decreasing lead time, with the 14 June forecasts typically placing the block too far

to west over the ocean (Fig. 3i). Further research is needed to investigate this response and determine if bias-correction can help improve sub-seasonal forecasts of blocking and associated extreme temperatures.

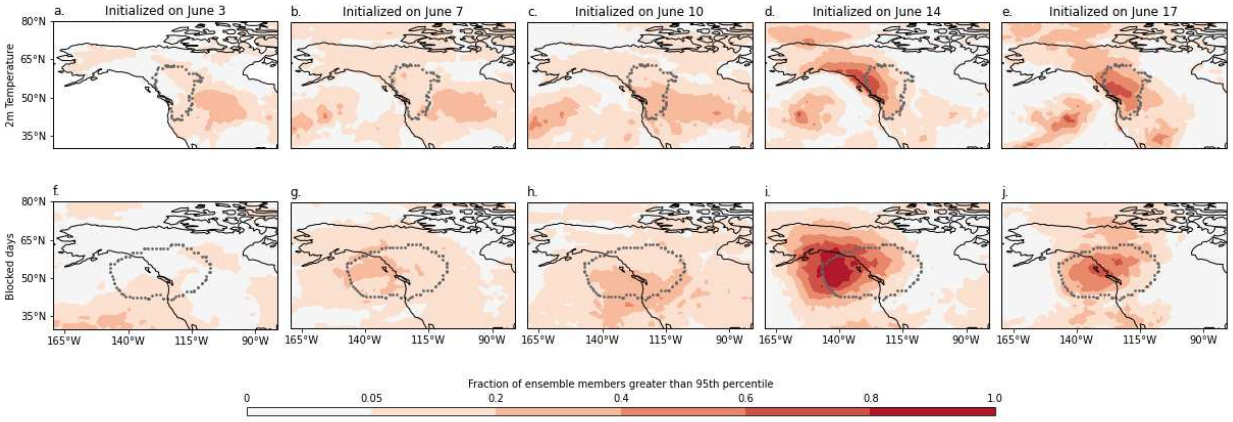

Figure 3. Fraction of ensemble members that predicted 2 m temperature (a-e) and number of blocked days (f-j) greater than the 95th percentile of the respective climatologies during 25 June to 1 July. For a 95th percentile event, 0.05 is the statistically expected value if there is no forecast skill. Forecasts initialized on 3 June (a,f), 7 June (b,g), 10 June (c,h), 14 June (d,i) and 17 June (e,j). Gray contours show the observed location of the heatwave based on ERA-5 reanalysis data.

Climate change context

What is the role of anthropogenic climate change in the severity or likelihood of this event? This is one of the first questions asked by the public and policy-makers alike. Despite recent progress in extreme event attribution science [9], this is a difficult question to answer for extremely rare events. One common approach is to quantify the change in the return period of an event; however, the validity of this method is uncertain for events this rare, as discussed in the pre-print by Philip et al (2021) [10] and corresponding referee comments.

It is clear, however, that anthropogenic warming of the planet contributed to the severity of this event – mean global temperatures for 2000-2020 were around 1°C warmer than in 1850-1900, largely attributable to anthropogenic emissions [11]. Land temperatures have warmed faster than the global mean (1.5°C since 1850-1900), and the rate of warming has increased over the past 70 years[11], increasing the probability of record-shattering extremes [12]. In the Pacific Northwest, mean summertime (JJA) temperatures have increased by 1.4°C from 1875-2020, suggesting that this event was approximately 1.4°C warmer than if an equivalent event had occurred at the end of the 19th century (see Methods). Changes in extremes may not necessarily mirror changes in the mean however [13] , and increases in JJA mean daily maximum temperatures were 0.5°C over this period. Aerosol emissions over the 20th century likely reduced the increase in extreme temperatures [14]. The rate of increase of extreme temperatures has quickened in the past 70 years (see Methods), consistent with aerosol emission reductions; this increasing trend is likely to continue in future decades [15].

Given that so many locations broke records by far more than the changes in temperatures discussed above, the question remains whether there was a dynamical impact of climate change on this event; the concerning possibility is that anthropogenic climate change may have made the atmospheric circulation patterns that led to this event more likely due to changes in the atmospheric dynamics. This is an area of on-going research and we are still far from full understanding and community consensus.

One proposed hypothesis is that Arctic amplification (AA), by reducing the equator-to-pole temperature gradient, reduces the strength of the mid-latitude atmospheric jetstream, which could lead to amplified mid-latitude atmospheric waves associated with heatwaves[16] There is significant disagreement in the scientific community regarding this hypothesis [17,18]. To investigate if AA-induced changes to atmospheric dynamics may have increased the probability of this extreme heatwave, we perform analysis on simulations from the Polar Amplification Model Intercomparison Project (PAMIP) [19]. The PAMIP simulations have been shown to simulate a weakening of the high-latitude jet in response to AA [20]; however, we find no evidence for robust changes in waviness over North America in response to sea ice loss or SST changes in two PAMIP models (those with available daily data; see Methods). Imposing sea ice loss alone misses other aspects of the AA response to anthropogenic warming [21]. Changes in Rossby wave sources due to changing diabatic heating in the tropics or in the extratropics, associated with drying soils in the mid-latitudes, may be another mechanism through which climate change can impact the dynamics of heatwaves [22]; further research in this critical research field is crucial.

Impacts

The impacts of the heatwave were felt across many spheres of our ecosystem. Whilst the extreme high temperatures lasted for around a week (Fig. 1b), some impacts continued long after. We provide analysis of a number of these impacts in their chronological order. We start with those felt mostly during the unprecedented heatwave, including human health impacts and coastal marine die-offs. Next, we consider impacts that were initiated during the heatwave but continued to be felt for weeks to months after, including wildfires, effects on agriculture and crops, snow/glacier melt and streamflow. Finally, we end with the landslides that occurred through summer and fall 2021 influenced by cascading effects initiated by the heatwave.

Human health impacts

Heatwaves can have catastrophic impacts on human health. Substantial increases in death rates have been documented during and immediately following past heatwaves, such those occurring in Chicago in 1995 [23], Western Europe in 2003 [24], and Moscow in 2010 [4]. During this 2021 heatwave, increased mortality was reported in BC and AB and the US states of WA, OR, and Idaho (ID) (see Methods for data sources). Whilst estimates of the total number of deaths due to this heatwave are likely to change over time as the event receives further study, evidence suggests that the death toll has little precedent in the affected regions, particularly BC. Between 25 June and 2 July, an estimated 740 excess deaths in the province were observed[1],

a 95% increase in population mortality over an 8-day period. Many of these deaths were reported to the BC Coroners Service, which has so far directly attributed 526 to extreme heat during the week of 25 June through 1 July [25]. Further mortality following the extreme heatwave has not yet been well-quantified, but it was likely the deadliest weather event in Canadian [1] and WA[26] history.

Most deaths during the heatwave occurred in private residences [25,26], likely due to dangerously high indoor temperatures [27]. Initial analyses of the community deaths in metropolitan Vancouver (the largest city in BC) found that they were disproportionately in neighborhoods with higher material and social deprivation and lower levels of green space [27], with higher risk among those aged 65-84 years and among females. Initial analyses also document that severe mental illness and substance use disorder were significant risk factors [28].

Serious but non-fatal health impacts also occurred. From 25-30 June the average daily number of emergency department visits for heat-related illnesses in WA, OR, ID , and Alaska was 69 times higher in 2021 than during the equivalent days in 2019, with disproportionate impacts on males and persons aged 75 and older [29]. WorkSafe BC, an agency dedicated to promoting safe and healthy workplaces across the province, advised employers to consider workplace closures during the extreme heat event, with numerous businesses following this advice.

From a public health perspective, it is important to reflect on the fact that the heatwave occurred after 18 months of a global pandemic. Social isolation is a known risk factor for heat related deaths [30,31], and there is ample evidence that social isolation increased drastically during the pandemic, especially among older adults [32]. As such, the COVID-19 pandemic response likely primed the most at-risk population to be particularly susceptible to this extreme heat event. It is also possible that some susceptible people avoided interventions such as cooling centres due to perceived COVID-19 risk.

Marine Life

Rocky intertidal shores are some of the most physically stressful habitats on Earth, and the species that occupy them often live very close to their physiological tolerance limits [33]. Intertidal ecosystems are therefore often used as bellwethers for the ecological effects of climate change and extreme weather events [34]. Plants and animals that live in the intertidal zone are especially susceptible to extreme high temperatures during daytime low tides, when solar insolation can raise organismal body temperatures well above air temperature [34,35]. The hottest days of the 2021 heatwave coincided with very low, early afternoon low tides throughout most of the Salish Sea (the inland waters of BC and WA). As a result, temperatures in excess of 50°C were observed in the intertidal zone (Fig. 4), particularly on gently sloping south and west facing surfaces that received the most direct solar radiation.

As the lethal thermal limits for even the most tolerant local intertidal species are well below 50°C, there was extensive mortality for numerous species at low tide. Species affected included barnacles, mussels, oysters, clams, gastropods, crabs, sea stars, and more (Fig. 4). Sessile species, which are unable to retreat to cooler microhabitats, were especially adversely

impacted. Barnacle and mussel mortality, accompanied by a very noticeable foul odor, was reported by researchers and concerned citizens from the southern end of Puget Sound, WA, to the BC Central Coast. Mortality was particularly pronounced in the Strait of Georgia, where temperatures were especially high and low tides were centered in the middle of the afternoon.

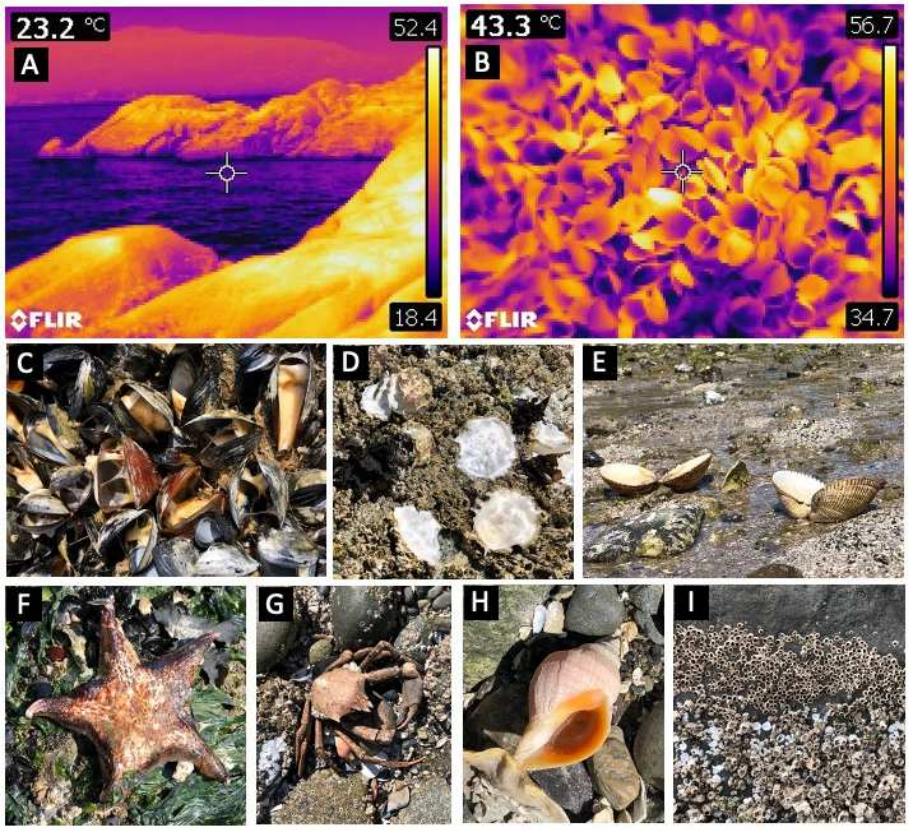

Figure 4. Impacts on marine life. (A,B) Thermal images showing extreme high temperatures on a rocky intertidal shoreline (A) and within a mussel bed (B) during low tide on 28 June, 2021. Scale bars indicate the range in temperature from the coolest to warmest parts of the image, while the value at the upper left indicates the temperature in the cross-hairs at centre. Note that the mussels in (B) have died and are gaping open. Panels C-I show a subset of species that were impacted by the heatwave, including (C) bay mussels, Mytilus trossulus, (D) Pacific oysters, Magallana (= Crassostrea) gigas, (E) heart cockles, Clinocardium nuttallii, (F) leather stars, Dermasterias imbricata, (G) kelp crabs, Pugettia producta, (H) dogwhelks, Nucella lamellosa, and (I) barnacles, Chthamalus dalli (upper portion of image) and Balanus glandula (lower portion of image). See methods for locations and dates of photos C-I.

On one representative mussel-dominated shoreline, the mussel (*Mytilus trossulus*) mortality rate was in excess of 70%, and over one million mussels were estimated to have died in a mere 100-m stretch of shoreline (see Methods). Surveys on a barnacle-dominated shoreline documented barnacle mortality rates that were also in excess of 70%; at this site, the heatwave killed roughly 10 million barnacles (*Balanus glandula*) along a single 100-m stretch of intertidal habitat (see Methods). While precise estimates for total heatwave-induced mortality along the highly heterogeneous ~7,500 km coastline of the Salish Sea are difficult to make, similar

magnitudes of proportional barnacle and mussel mortality were widely observed, and the total number of marine invertebrates killed was almost certainly in the billions.

Wildfires

The persistent hot and dry conditions associated with the heatwave cured forest vegetation, resulting in extreme fire danger and increased wildfire activity. Figure 5 shows the increase in Fire Weather Index (FWI; see Methods), modeled smoke concentration, and satellite-detected hotspots from 20 June (pre-heatwave) and 3 July (post-heatwave). Over this period, BC went from six active wildfires with 123.5 hectares burned to 175 wildfires consuming 78,939 hectares. On 30 June, observed FWI values in Lytton, BC, reached an extraordinary value of 132. By 11 July, the Canadian Interagency Forest Fire Centre (CIFFC) increased Canada's National preparedness level to 5, its highest rank: wildfire suppression resources were limited, and aid from international agencies was requested.

During the heatwave itself, two noteworthy fires were discovered actively burning within the BC Southern Interior: the Sparks Lake Fire (discovered 28 June), and the McKay Creek Fire (discovered 29 June). Both are suspected to be human-caused, and were located in the Southwest Interior of BC, a zone that experienced some of the hottest and driest conditions throughout the heatwave. On the afternoon of 29 June, mid-tropospheric moisture moved into the high pressure ridge, helping produce the thermodynamics for pyrocumulonimbus flammagenitus (CbFg) clouds to form over these burning wildfires. These CbFg clouds can produce large amounts of lightning, providing ignition for more fires [36,37]. Combustion of the forest vegetation produces smoke particles and releases additional water vapour into strong thermal updrafts above wildfires [36]. The combined smoke and water vapour rise to cloud base, where they cool and condense into cloud droplets; this led to the development of CbFgs over each wildfire in the late afternoon on 29 and 30 June. On 30 June, the CbFgs were highly convective, producing positively charged anvil cloud tops that propagated northward (as determined from GOES-17 visible satellite imagery). Over the evening hours of 30 June, approximately 120,800 cloud-to-ground lightning strikes occurred [38], with the CIFFC reporting at least 127 new lightning-ignited wildfires from 30 June to 2 July.

The high pressure ridge began to break down around 30 June. This led to additional hot, dry, and now windy and unstable conditions, which fanned the flames of wildfires ignited by the CbFg lightning and enabled rapid growth of these fires. The continued breakdown of the ridge and a cold frontal passage yielded more CbFgs and lightning with little precipitation. This cycle occurred each afternoon during the first week of July and ignited on average 40 new wildfires each day.

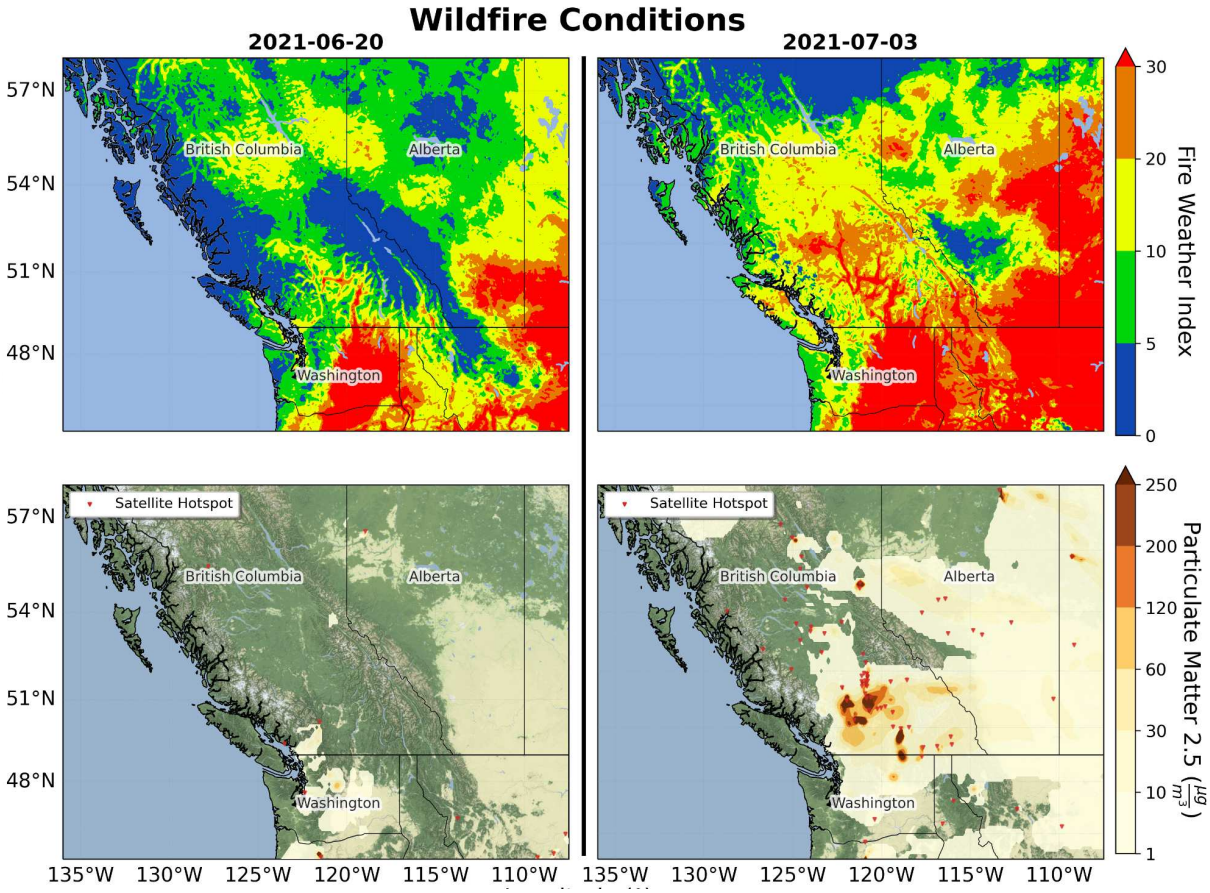

Figure 5. Top row: model estimated Fire Weather Index (FWI). Bottom row: smoke concentration as represented by the concentration of Particulate Matter (PM) 2.5 and satellite hotspots. Left column is for 20 June (pre-heatwave); right column is 3 July (post-heatwave).

Agriculture

The heatwave had pronounced impacts on agriculture in BC and AB, notably occurring during crucial growing stages of many crops. The BC agricultural sector generates $3.9B in farm value and encompasses over 2.6M hectares of farmland, with the highest diversity of crops in Canada [39]; whilst in Alberta agriculture encompasses 25.3M hectares with a farm value of $15.4B [40]. BC also produces more fruit than any other province in Canada [39]. Extreme weather events such as heatwaves can severely impact annual yields[41]—when temperatures exceed a crop-dependent threshold substantial drops in yield result [42]. We compare 2021 annual crop and fruit yield estimates (e.g., kilograms of crop per hectare harvested) to the 2011-2020 average. It is extremely difficult to isolate the impacts of one particular event on annual yield data however; thus we also use weekly resolution, satellite-derived Normalized Difference Vegetation Index (NDVI; see Methods) to analyse the timing of changes in crop greenness relative to the heatwave.

Estimates of 2021 yields for major BC field crops were substantially lower than 10-year averages, with tame hay reduced by 32%, canola by 18%, spring wheat by 35% and barley by 30%. An exception to these yield declines was oats, with 2021 yields only 5% below the 10-year

average. Similar yield declines were seen in AB, with many field crop yields the lowest since the widespread drought of 2002, including tame hay (35% lower than the 10-year average), canola (31%), spring wheat (31%), barley (32%) and oats (23%).

In 6 out of the 8 BC agricultural divisions a noticeable drop in NDVI occurred during the heatwave period (Fig. 6), with the strongest impacts in the Kootenay and Thompson-Okanagan regions of interior BC; the latter region includes the town of Lytton (shown in Fig. 1a). In these two regions the NDVI dropped from climatological mean values before the heatwave, to more than 2 standard deviations below the mean by mid-July, and remained at extremely low levels until August (Julian weeks 31-35). The timing of these decreases suggests that this unprecedented heatwave likely played a significant role in the annual yield declines.

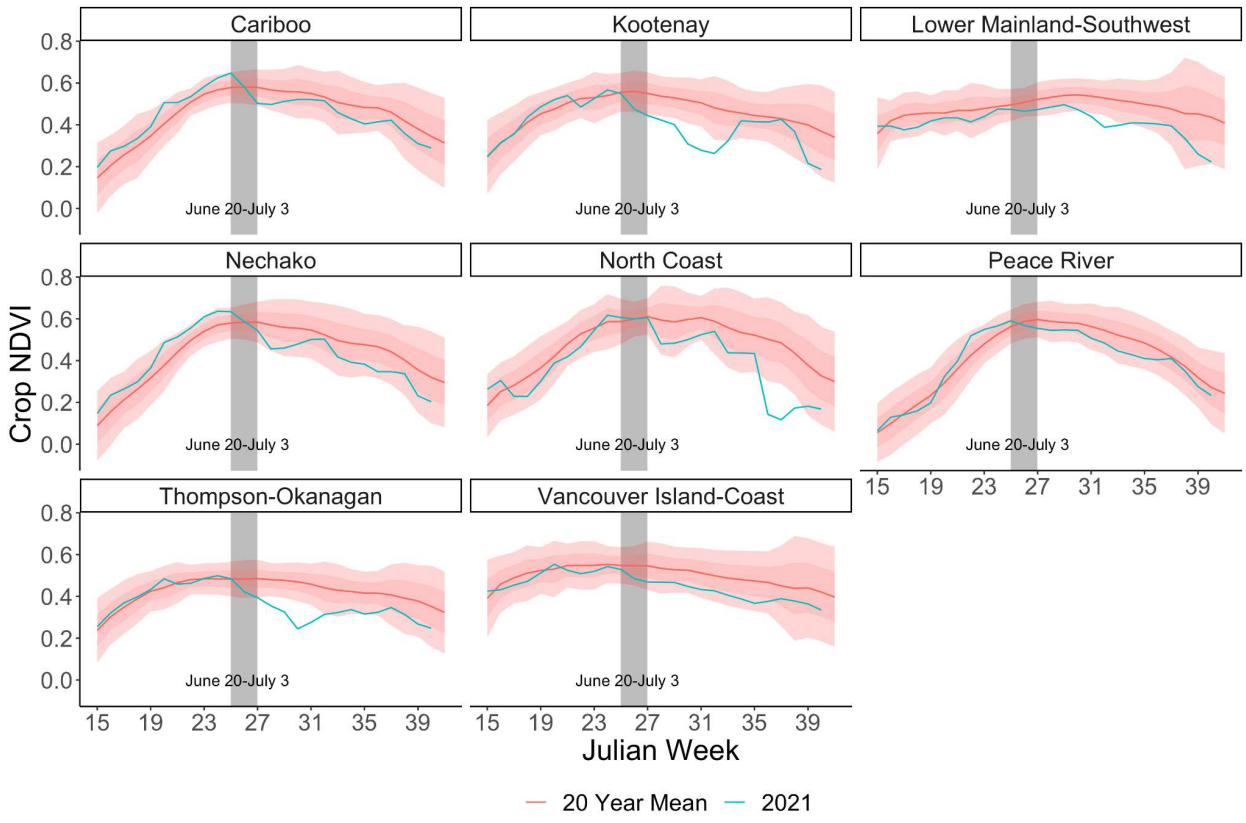

Figure 6. Weekly NDVI from the Crop Condition Assessment Program (see methods), spatially averaged over agricultural divisions in BC, organized alphabetically. Blue line shows 2021, red line the 2000-2020 mean, and shading shows interannual variability (+/- 1 and 2 standard deviations). The grey highlighted region shows the heatwave period, 20 June - 3 July; data is reported as weekly averages and so the heatwave is split between weeks 20-26 June and 27 June - 3 July.

The production of many major fruit crops also faced major declines in 2021, with yields lower than the 10-year average for blueberries (by 10%), sweet cherries (39%), grapes (19%), apples (12%) and raspberries (39%). Cranberry yields were 10% above the 10-year average, which may be due to more intensive moisture management of a crop that has high irrigation coverage

compared to other fruits in the province. Vegetable yields also suffered in 2021 for many crops, including cabbage (10% lower than 10-year average), pumpkins (34%), and lettuce (12%), amongst others. The livestock sector in BC also experienced significant mortalities during the heatwave, with reportedly at least 651,000 farm animals dying between 24 June to 30 June [2].

Cryosphere and streamflow

The unprecedented heatwave had a pronounced influence on the region's cryosphere and hydrology both during the event, and for months after. The BC heatwave-induced streamflow response was spatially variable, in large part due to the variation in snowpack and glacier coverage throughout the province (see Supplemental Figure S2).

The exceptionally warm temperatures and clear sky conditions drove rapid ice and snow melt, leading to substantially increased streamflow in basins that had snow or ice available to melt (Fig. 7a-f). In many cases, daily record high flows were achieved, with some all-time records broken (Supplementary Fig. S3). The rapid increase in streamflow led to flood warnings for several downstream communities and an evacuation order in the Pemberton Valley. In some cases, melt rates and the rate of change of daily streamflow decreased during the heatwave due to snowpack depletion, despite continuing extreme temperatures (e.g. Fig 7d and f). While dry conditions persisted in many regions in the days following the heatwave, subsequent rainfall in the Rocky Mountains near the BC/AB border exacerbated flooding and damages [43], leading to substantial damages within BC's Mt Robson Provincial Park, and the helicopter evacuation of hikers [44].

Glacier melt is an important control of interannual summer streamflow variability [45,46]. The extensive snow melt during the heatwave exposed darker, lower-albedo glacier ice. Combined with persistent warm conditions through much of July this resulted in large amounts of seasonal glacier melt. While basins without substantial glacier coverage experienced lower than normal flows (Fig. 7g-i), the influx of glacier meltwater in glaciated basins resulted in late summer streamflows similar to the historical average (Fig. 7 a-c), despite the substantial loss of snowpack during the heatwave. The ability of glaciers to sustain normal flows is notable considering the unprecedented nature of the heatwave, and came at the cost of substantial glacier mass loss [47]. The ability of glaciers to compensate for such extreme events is expected to diminish in the future with continued climate change[48].

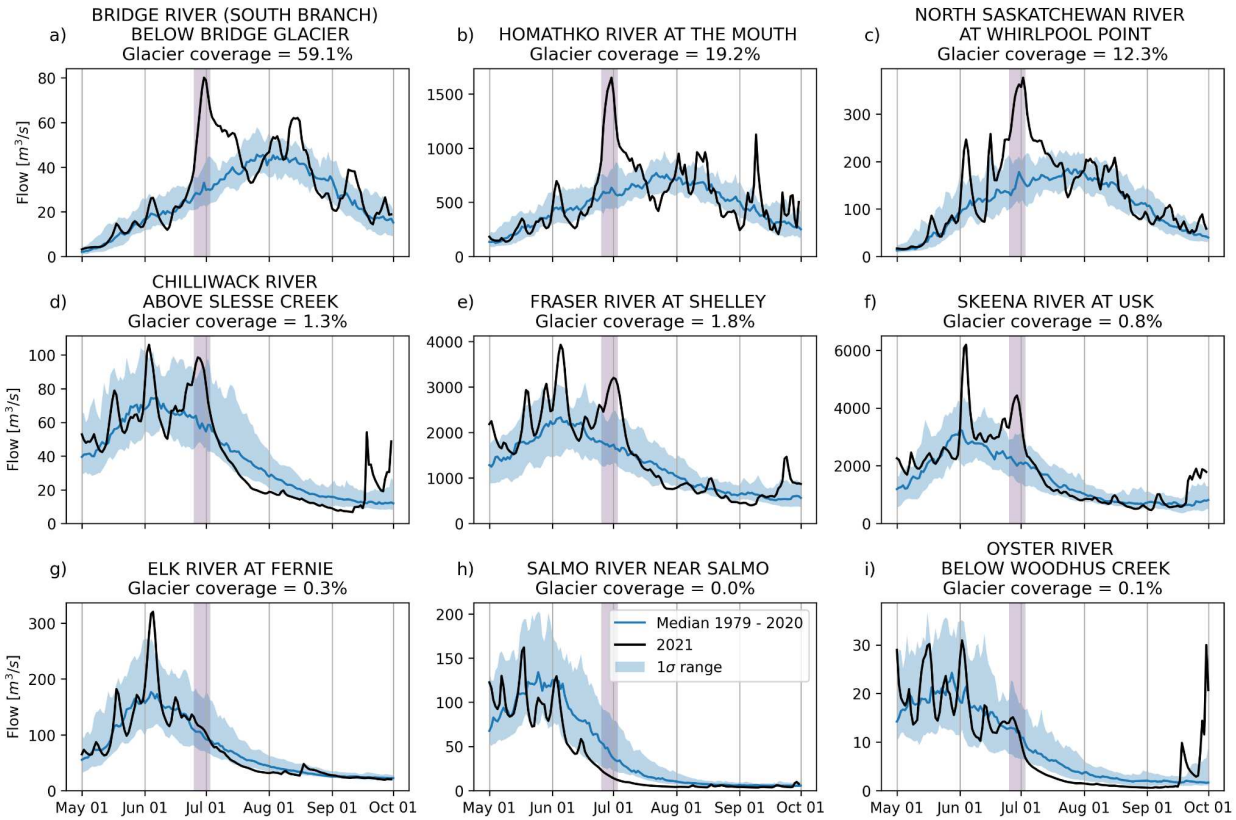

Figure 7. Streamflow observations at nine stream gauge stations in 2021 (black line) relative to the 1979-2020 median (blue line) and 1 standard deviation range (shaded). (a) - (c) Highly glaciated basins; (d) - (f) Lightly glaciated basins; (g) - (i) Minimally or non-glaciated basins.

Landslides

Wildfires can result in an increased risk of flooding, erosion and landslides, due to impacts on both vegetation and soil [49]. Such impacts include reduction of infiltration rate and water storage capacity, an increase in the susceptibility of the soil to erosion by raindrops, and in some cases increased water repellency of the soil below the surface [49,50]. These changes increase the susceptibility of slopes to debris flows, with studies showing that post-wildfire debris flows often occur in areas with moderate to high burn severity [49,51]. Processes associated with wildfires in BC during 2021 is twofold: the loss of vegetation and hydrophobicity of the soils led to a more pronounced stream runoff response with steeper hydrographs. Secondly, the added sediment charged the receiving rivers with excess sediment, locally aggrading channel beds and encouraging avulsions and bank erosion.

Hundreds of post-wildfire debris flows were triggered by rainstorms in the summer and fall of 2021 in southwestern BC (Supplementary Fig. S5). One of the largest wildfires associated with this heatwave was the Lytton Creek Fire, which began south of the village of Lytton and burned approximately 84,000 hectares [52]. In addition to the extensive damages to Lytton and Lytton First Nation reserves previously described, post-wildfire debris flows affected railway and highway infrastructure. On 16 August, debris flows impacted two semi-trailers and a car on the

TransCanada Highway, with no fatalities reported. Further post-wildfire debris flows that damaged infrastructure but did not impact vehicles occurred on 17 September, and during an extreme atmospheric river event on 14-15 November.

Debris flows following the 16 August rainstorm in the Nicoamen River watershed are shown in Fig. 8. Rainfall rates were not unusually heavy: 4-10 mm h^{-1} over approximately 4 hours, corresponding to a less than 2-year return period event in this region. The fire-related water repellency in the soil caused soil rilling and in-channel sediment mobilization, resulting in abundant sediment transport. Further rainfall in the Nicoamen River watershed during the atmospheric river on 14-15 November remobilized the debris flow sediment as part of a post-wildfire debris flood that undermined three bridge approaches on the TransCanada Highway and one building foundation, resulting in one bridge collapse and necessitating repairs on another. Outside of the Nicoamen River, post-wildfire debris flows and debris floods in the Lytton Creek Fire perimeter severed railway and highway infrastructure (bridges and embankments) in nine other locations[53]. This event likely resulted in the most expensive natural disaster in Canada's history, with millions of dollars worth of damage along southwest BC's highways and railways with bridges, railways, and highway embankments failing.

Figure 8. Post-wildfire debris flows in Nicoamen River triggered by a rainstorm on 16 August 2021. Severely burnt vegetation is shown by blackened trees. Debris flows originated as slope wash and rilling on steep burnt slopes. Extreme temperatures can also open desiccation cracks in fine-grained (clay and silt-rich) sediments. Those cracks can later allow ingress of rainwater to potential failure planes at depth which may exacerbate landslide hazards well after the heat waves and wildfires have ended.

Discussion

This event has been described as “the most anomalous regional extreme heat event to occur anywhere on Earth since temperature records began” [54]. The unprecedented nature of this event made it difficult to anticipate and mitigate its potential impacts. While forecast information was available, and efforts were made to communicate the severity of the event and reduce heat mortality, the consequences of this event indicate we must do better in future. BC is in the process of identifying extreme heatwaves as ‘Extreme Heat Emergencies’, producing alerts analogous to similar systems for wildfires and flooding. The intention is to provide an appropriately coordinated and resourced provincial response when the next event occurs. The extraordinary nature of this extreme heatwave highlights that all jurisdictions should now be working to address the inevitable risk of unprecedented heat.

As we move into an unrelentingly warmer world due to anthropogenic global warming, extreme heat events across the globe are becoming increasingly common and more intense [12,55]. Many of the negative effects of this heatwave were disproportionately felt by First Nations people across BC, the elderly, and people living in neighbourhoods with higher material and social deprivation, highlighting the importance of climate justice in the response to climate change[56].

The catastrophic impacts of this unprecedented heatwave underscore the importance of understanding extreme weather events and how their frequency or intensity will change with anthropogenic climate change, and crucially, how to mitigate their impacts. Raju et al. (2022) [57] argue that disasters occur when hazards meet vulnerability, and that we can, and should, work to reduce both the hazards (through reducing anthropogenic climate change) and the vulnerability (through changing social and political processes). This heatwave has provided lessons and examples that we can learn from. It provides us with a vivid depiction of why and how climate change can be so devastating. It is imperative that we listen, and learn, from what nature has to tell us.

References

All website pages and reports cited in this paper have been archived using the Internet Archive Wayback Machine (https://archive.org/) in case they become unavailable from the original source.

1. Henderson, S. B., McLean, K. E., Lee, M. J. & Kosatsky, T. Extreme heat events are public health emergencies. *BC Medical Journal* **63**, 366–367 (2021).
2. Environment and Climate Change Canada. Canada's top 10 weather stories of 2021. https://www.canada.ca/en/environment-climate-change/services/top-ten-weather-stories/2021.html (2022).
3. Robine, J.-M. *et al.* Death toll exceeded 70,000 in Europe during the summer of 2003. *C. R. Biol.* **331**, 171–178 (2008).
4. Shaposhnikov, D. *et al.* Mortality related to air pollution with the moscow heat wave and wildfire of 2010. *Epidemiology* **25**, 359–364 (2014).
5. Overland, J. E. Causes of the Record-Breaking Pacific Northwest Heatwave, Late June 2021. *Atmosphere* **12**, 1434 (2021).
6. Pfahl, S. & Wernli, H. Quantifying the relevance of atmospheric blocking for co-located temperature extremes in the Northern Hemisphere on (sub-)daily time scales. *Geophys. Res. Lett.* **39**, L12807 (2012).
7. Brewer, M. C., Mass, C. F. & Potter, B. E. The West Coast Thermal Trough: Climatology and Synoptic Evolution. *Mon. Weather Rev.* **140**, 3820–3843 (2012).
8. Lin, H., Mo, R. & Vitart, F. The 2021 western North American heatwave and its subseasonal predictions. *Geophys. Res. Lett.* (2022) doi:10.1029/2021gl097036.
9. van Oldenborgh, G. J. *et al.* Pathways and pitfalls in extreme event attribution. *Clim. Change* **166**, 13 (2021).
10. Philip, S. Y. *et al.* Rapid attribution analysis of the extraordinary heatwave on the Pacific Coast of the US and Canada June 2021. (2021) doi:10.5194/esd-2021-90.
11. Gulev, S. K. *et al.* Changing State of the Climate System. in *Climate Change 2021: The Physical Science Basis. Contribution of Working Group I to the Sixth Assessment Report of the Intergovernmental Panel on Climate Change* (eds. Masson-Delmotte, V. et al.) (Cambridge University Press (in press), 2021).
12. Fischer, E. M., Sippel, S. & Knutti, R. Increasing probability of record-shattering climate extremes. *Nat. Clim. Chang.* **11**, 689–695 (2021).
13. McKinnon, K. A., Rhines, A., Tingley, M. P. & Huybers, P. The changing shape of Northern Hemisphere summer temperature distributions. *J. Geophys. Res.* **121**, 8849–8868 (2016).
14. Mascioli, N. R., Fiore, A. M., Previdi, M. & Correa, G. Temperature and Precipitation Extremes in the United States: Quantifying the Responses to Anthropogenic Aerosols and Greenhouse Gases. *J. Clim.* **29**, 2689–2701 (2016).
15. Samset, B. H. *et al.* Climate Impacts From a Removal of Anthropogenic Aerosol Emissions. *Geophys. Res. Lett.* **45**, 1020–1029 (2018).
16. Francis, J. A. & Vavrus, S. J. Evidence linking Arctic amplification to extreme weather in mid-latitudes. *Geophys. Res. Lett.* **39**, (2012).
17. Cohen, J. *et al.* Divergent consensuses on Arctic amplification influence on midlatitude severe winter weather. *Nat. Clim. Chang.* **10**, 20–29 (2020).

18. Stendel, M., Francis, J., White, R. H., Wiliams, P. D. & Woollings, T. The Jet Stream and Climate Change. in *Climate Change - Observed Impacts on Planet Earth* (ed. Letcher, T.) 327–357 (Elsevier, 2021).
19. Smith, D. M. *et al.* The Polar Amplification Model Intercomparison Project (PAMIP) contribution to CMIP6: investigating the causes and consequences of polar amplification. *Geosci. Model Dev.* **12**, 1139–1164 (2019).
20. Smith, D. M. *et al.* Robust but weak winter atmospheric circulation response to future Arctic sea ice loss. *Nat. Commun.* **13**, 727 (2022).
21. Labe, Z., Peings, Y. & Magnusdottir, G. Warm arctic, cold Siberia pattern: Role of full arctic amplification versus sea ice loss alone. *Geophys. Res. Lett.* **47**, (2020).
22. Teng, H. & Branstator, G. Amplification of Waveguide Teleconnections in the Boreal Summer. *Current Climate Change Reports* **5**, 421–432 (2019).
23. Whitman, S. *et al.* Mortality in Chicago attributed to the July 1995 heat wave. *Am. J. Public Health* **87**, 1515–1518 (1997).
24. Pirard, P. *et al.* Summary of the mortality impact assessment of the 2003 heat wave in France. *Euro Surveill.* **10**, 153–156 (2005).
25. British Columbia Coroners Service. *BC Coroners Service (BCCS) Heat-Related Deaths – Knowledge Update*. https://www2.gov.bc.ca/assets/gov/birth-adoption-death-marriage-and-divorce/deaths/coroners-service/statistical/heat_related_deaths_in_bc_knowledge_update.pdf (2021).
26. Washington State Department of Health. Heat Wave 2021. https://doh.wa.gov/emergencies/be-prepared-be-safe/severe-weather-and-natural-disasters/hot-weather-safety/heat-wave-2021 (2021).
27. Henderson, S. B., McLean, K. E., Lee, M. J. & Kosatsky, T. Analysis of community deaths during the catastrophic 2021 heat dome: Early evidence to inform the public health response during subsequent events in greater Vancouver, Canada. *Environ Epidemiol* **6**, e189 (2022).
28. Henderson, S. Mortality during the catastrophic 2021 heat dome: What we know and where we need to go. https://nexuswebcast.mediasite.com/mediasite/Showcase/bc-cdc-showcase/Presentation/896ca6fb39e246ab801c0526867b73741d (2021).
29. Schramm, P. J. *et al.* Heat-Related Emergency Department Visits During the Northwestern Heat Wave - United States, June 2021. *MMWR Morb. Mortal. Wkly. Rep.* **70**, 1020–1021 (2021).
30. Kafeety, A. *et al.* Social connection as a public health adaptation to extreme heat events. *Can. J. Public Health* **111**, 876–879 (2020).
31. Orlando, S. *et al.* The Effectiveness of Intervening on Social Isolation to Reduce Mortality during Heat Waves in Aged Population: A Retrospective Ecological Study. *Int. J. Environ. Res. Public Health* **18**, (2021).
32. Sayin Kasar, K. & Karaman, E. Life in lockdown: Social isolation, loneliness and quality of life in the elderly during the COVID-19 pandemic: A scoping review. *Geriatr. Nurs.* **42**, 1222–1229 (2021).
33. Helmuth, B., Mieszkowska, N., Moore, P. & Hawkins, S. J. Living on the Edge of Two Changing Worlds: Forecasting the Responses of Rocky Intertidal Ecosystems to Climate Change. *Annu. Rev. Ecol. Evol. Syst.* **37**, 373–404 (2006).

34. Harley, C. D. G. Tidal dynamics, topographic orientation, and temperature-mediated mass mortalities on rocky shores. *Mar. Ecol. Prog. Ser.* **371**, 37–46 (2008).
35. Helmuth, B. S. T. Intertidal mussel microclimates: Predicting the body temperature of a sessile invertebrate. *Ecol. Monogr.* **68**, 51–74 (1998).
36. Rosenfeld, D. *et al.* The Chisholm firestorm: observed microstructure, precipitation and lightning activity of a pyro-cumulonimbus. *Atmos. Chem. Phys.* **7**, 645–659 (2007).
37. Tory, K. J., Thurston, W. & Kepert, J. D. Thermodynamics of Pyrocumulus: A Conceptual Study. *Mon. Weather Rev.* **146**, 2579–2598 (2018).
38. Vagasky, C. Pyrocumulonimbus event in British Columbia, Canada. https://www.vaisala.com/en/blog/2021-07/pyrocumulonimbus-event-british-columbia-canada (2022).
39. BC Ministry of Agriculture – Statistics and Corporate Program Management Unit. *Sector Snapshot 2019: B.C. Agriculture*. https://www2.gov.bc.ca/assets/gov/farming-natural-resources-and-industry/agriculture-and-seafood/statistics/industry-and-sector-profiles/sector-snapshots/sector_snapshot_2019_-_agriculture.pdf (2019).
40. Alberta Agriculture and Forestry. *Agriculture Statistics Factsheet*. https://open.alberta.ca/dataset/79f01912-5e5c-469e-8cf4-97cfc6901cea/resource/745669c0-cba5-449d-b1a3-0402fa015d8c/download/af-itrb-agriculture-statistics-factsheet-2020.pdf (2020).
41. Lesk, C., Rowhani, P. & Ramankutty, N. Influence of extreme weather disasters on global crop production. *Nature* **529**, 84–87 (2016).
42. Schlenker, W. & Roberts, M. J. Nonlinear temperature effects indicate severe damages to U.S. crop yields under climate change. *Proc. Natl. Acad. Sci. U. S. A.* **106**, 15594–15598 (2009).
43. BC River Forecast Centre. *Flood Warning – Upper Fraser River (UPGRADED)*. http://bcrfc.env.gov.bc.ca/warnings/advisories/FWN_2021_06_29_1300UpperFraser_iss.pdf (2021).
44. Roffel, B. Famed B.C. hiking trail to remain closed for rest of 2021 because of flooding damage. *CBC News* (2021).
45. Fountain, A. G. & Tangborn, W. V. The effect of glaciers on streamflow variations. *Water Resour. Res.* **21**, 579–586 (1985).
46. Anderson, S. & Radić, V. Identification of local water resource vulnerability to rapid deglaciation in Alberta. *Nat. Clim. Chang.* **10**, 933–938 (2020).
47. Menounos, B. *et al.* Cryospheric response to the June, 2021 Heat Dome. in *AGU Fall Meeting 2021* (AGU, 2021).
48. Clarke, G. K. C., Jarosch, A. H., Anslow, F. S., Radić, V. & Menounos, B. Projected deglaciation of western Canada in the twenty-first century. *Nat. Geosci.* **8**, 372–377 (2015).
49. Jordan, P. & Ashley Covert, S. Debris Flows and Floods Following the 2003 Wildfires in Southern British Columbia. *Environ. Eng. Geosci.* **15**, 217–234 (2009).
50. Shakesby, R. A. & Doerr, S. H. Wildfire as a hydrological and geomorphological agent. *Earth-Sci. Rev.* **74**, 269–307 (2006).
51. Gartner, J. E., Cannon, S. H., Santi, P. M. & Dewolfe, V. G. Empirical models to predict the volumes of debris flows generated by recently burned basins in the western U.S. *Geomorphology* **96**, 339–354 (2008).

52. BC Wildfire Service. Wildfire season summary. https://www2.gov.bc.ca/gov/content/safety/wildfire-status/about-bcws/wildfire-history/wildfire-season-summary (2021).
53. Lau, C.-A. *et al.* Hydro-geomorphic effects of the November 2021 atmospheric rivers on infrastructure in Southwestern British Columbia. in *Geohazards 8: Proceedings of the 8th Canadian Conference on Geotechnique and Natural Hazards. Quebec, Canada* (2022).
54. Henson, B. & Masters, J. Western Canada burns and deaths mount after world's most extreme heat wave in modern history. *Yale Climate Connections* https://yaleclimateconnections.org/2021/07/western-canada-burns-and-deaths-mount-after-worlds-most-extreme-heat-wave-in-modern-history/ (2021).
55. Seneviratne, S. I. *et al.* Weather and Climate Extreme Events in a Changing Climate. in *Climate Change 2021: The Physical Science Basis. Contribution of Working Group I to the Sixth Assessment Report of the Intergovernmental Panel on Climate Change* (eds. Masson-Delmotte, V. et al.) (Cambridge University Press (in press), 2021).
56. Newell, P., Srivastava, S., Naess, L. O., Torres Contreras, G. A. & Price, R. Toward transformative climate justice: An emerging research agenda. *Wiley Interdiscip. Rev. Clim. Change* **12**, (2021).
57. Raju, E., Boyd, E. & Otto, F. Stop blaming the climate for disasters. *Communications Earth & Environment* **3**, 1–2 (2022).

Author Contributions

Rachel H. White coordinated the contributions, and wrote the overview, discussion, and climate change context sections, and contributed to the subseasonal forecasts section. Rachel H. White and Christopher Rodell came up with the initial idea for the paper. Greg West wrote the synoptic conditions and forecasts sections; Lualawi Mareshet Admasu, James F. Booth, and Veeshan Narinesingh performed analysis for, and contributed to, the subseasonal forecast section; Cuiyi Fei and Eliott Roocroft performed analysis for the climate change context section, and Eliott Roocroft helped create Figs. 1 and 2. Sarah B. Henderson and Kate R. Weinberger provided the human health section, and contributed to the discussion; Christopher D. G. Harley contributed the marine life section; Chris Rodell contributed the wildfires sections; Ginni Braich contributed the agriculture section; Sam Anderson and Christina Draeger contributed the cryosphere and streamflow section; Carie-Ann Lau and Matthias Jakob contributed the landslides section.

Acknowledgements

Intertidal surveys were conducted on the traditional, ancestral, and unceded territories of the Coast Salish peoples. Landslide studies were done on the traditional territories of the Nłeʔkepmx Tmíxʷ (Nlaka'pamux) First Nations including member nations of the Nlaka'pamux Tribal Council, Scw'exmx Tribal Council, and the Lytton First Nation.
RHW, LMA, CF and ER acknowledge support from the Natural Sciences and Engineering Research Council of Canada (NSERC) [RGPIN-2020-05783]. GW acknowledges support from BCHydro. CR acknowledges support from:NSERC, MITACS, BCHydro, Natural Resources Canada, Government of British Columbia Ministry of Environment and Climate Change

Strategy, Government of Alberta Environment and Sustainable Resource Development, Government of the Northwest Territories Environment and Natural Resources. GB was funded by the Alberta Innovates Grant 2019F163R. SA was funded by an NSERC doctoral scholarship. CDGH was supported by an NSERC Discovery Grant [RGPIN-2016-05441]. C-AL and MJ acknowledge contributions of locations of post-wildfire debris flow observations from the Ministry of Forests, Lands, Natural Resource Operations and Rural Development and Canadian Pacific Railway.

Methods

Event overview

To compare the record temperature exceedance to previous heatwaves we used gridded daily maximum 2*m* temperatures (T2m) from 1950-2021 from the ERA5 reanalysis data [58], which assimilates observations. The data from 1950-1978 are preliminary, but quality concerns are restricted to tropical cyclones. A previous version of the ECMWF reanalysis, ERA-interim, performs well relative to pure-observational datasets for temperature extremes [59] and thus we expect ERA5 to provide a reasonably accurate assessment. Daily maximum temperatures are found from hourly maximum 2*m* temperature values. Data is downloaded from the C3S datastore [60,61] on a 1° x 1° spatial grid. Maximum daily maximum temperature is calculated for the heatwave period from 22 June - 3 July 2021, and for the 'historical' period from 1 January 1950 through to 1 June 2021. The difference between these is shown in Fig. 1, with the 2003 European heatwave (max T2m between 29 July - 16 August 2003 relative to max T2m from 1 January 1950 - 1 June 2003), and the 2010 Russian heatwave (max T2m between 1 July 2010 - 16 August 2010 relative to max T2m from 1 January 1950 - 1 June 2010. For comparison, we repeat the analysis with maximum daily maximum temperature and maximum daily minimum temperature from 1951-2021 using the monthly Gridded Temperature and Precipitation Climate Extreme Indices dataset (GHCNDEX) [62]. These plots, with similar results, are shown in Supplementary Fig. S1.

In Fig. 1b we include the same temperature exceedance for observations (shown in the individual markers) from the Canadian Long Term Climate Extremes database, created by the Meteorological Service of Canada [63]. For this dataset "virtual" climate stations were created by joining together climate data from stations nearby to make long-term records, allowing for longer records than looking at individual stations. We show data only for virtual stations that go back to at least 1949, with the longest record starting in 1874. Note that these data have not been quality controlled to remove artifacts such as discontinuities and non-climate trends; however, the dataset is updated frequently, allowing us to use it for recent events. We expect the 'record exceedance' values from individual stations to be slightly lower than for the ERA5 dataset, as many of the records are longer; this can be seen in Fig. 1a. The general extent and distribution of the record exceedances are similar, with close agreement over the station of Lytton, shown in the triangle, where the new Canadian daily record maximum temperature was set.

Synoptic conditions

The description of the synoptic conditions was produced through analysis of the evolution of geopotential height, wind speed, precipitable water, relative humidity, temperature, and sea-level pressure fields, at various levels in the atmosphere. In Fig. 2 temperature values are daily averages of 6-hourly data, with anomalies relative to a daily 1980-2020 climatology, whilst geopotential heights are instantaneous values at 1200 UTC (0500 PDT); all data from the ERA5 reanalysis[58].

To gain insight into the processes responsible for the near-surface temperature extremes, 4-day backwards trajectories terminating within the boundary layer over the BC Southern Interior at

0000 UTC 28 June were calculated using the NOAA HYSPLIT model. Results are shown in Supplementary Fig. S4.

Forecasts

Over the past decade "ensemble" weather forecasting has become prevalent in operational forecast offices, particularly at the medium to long forecast horizons (~4-14 days into the future). A forecast ensemble contains many models, or "members," that typically have varied initial states and/or physics parameters. The benefits of this approach are twofold: 1) the mean or median of the ensemble forecasts, typically taken as the most likely outcome, is more accurate than a single model; and 2) the members sample the uncertainty space, thus giving users a sense of the range and probability of various outcomes. Statistical post-processing is typically applied to the raw ensemble output to improve the accuracy of both the mean/median, and the probabilities derived from the distribution of ensemble members.

We use forecast data from the 42-member North American Ensemble Forecast System (NAEFS) [64–66]. The NAEFS setup presented here has undergone bias correction and probabilistic calibration (similar to the methods described in Bourdin et al. 2014[67]), and is representative of the forecast skill of a typical modern medium-range operational forecast system.

Seasonal forecasts

This heatwave was characterized by record-breaking surface temperatures and a slowly propagating blocking high with extreme geopotential anomalies at 500-hPa (z500). Thus, to evaluate the subseasonal to seasonal (S2S) forecasts, we focus on probabilistic forecasts of 2-m air temperature (t2m) anomalies and frequency of blocking[68] observed over the days between 25 June and 1 July and compare to those in ERA5 data [58]. Soil moisture analysis was conducted using ERA5-land data[69].

We use the state-of-the-art ECMWF Integrated Forecasting System (IFS) model, one of 11 models available as part of the S2S prediction project database [70]. The IFS has 51 forecast ensemble members, with 11 reforecast members implemented over the previous 20 years, and has a maximum resolution of 0.5°. Previous evaluations of ECMWF indicate good performance up to lead times of 7-10 days for extreme cold events [71], up to 11 days for daily precipitation [72], up to 15 days for heatwaves [73,74] and up to 20 days for soil moisture [75].

To understand the prediction skill of ensemble forecasts for an extreme event we take a probabilistic approach [76]. We investigate the forecast skill in predicting 'an extreme', rather than necessarily an extreme of the magnitude observed. We show results for an extreme event defined as one exceeding the 95th percentile, but relatively similar results are obtained for the 90th and 99th percentiles. We identify the 95th percentile threshold for the variable of interest (temporally averaged t2m anomalies or number of blocked days) averaged over 25 June to 1 July across all reforecast years (2001-2020) and ensemble members. We then calculate the fraction of forecast ensemble members that predicted t2m anomalies or number of blocked days higher than this threshold for 25 June to 1 July 2021. Comparison to the expected value for a

climatological forecast (0.05 for the 95th percentile) gives the increased probability of the event as predicted by the ensemble forecast.

The model climatology, required to calculate anomalies, was calculated from the reforecast data using the methodology of Owens and Hewson (2018) [77]. This eliminates systematic biases of the forecasted weather relative to the climatology, and accounts for model drift due to changing lead times. The original methodology has a slight difference in the calculation of the climatology for lead times greater than, or less than, 15 days; for consistency across all lead times considered in this work, we calculate all climatologies using 5 consecutive reforecasts. The climatology is calculated for years 2001-2020. For consistency between models and reanalysis data, the ERA5 climatology is calculated using years 2001-2020 and smoothed using a 5-day running mean.

Blocking frequency was calculated based on a modified [78] version of the algorithm proposed by Dunn-Sigouin et al. (2012) [79,80]. For the algorithm to define a block, a persistent, positive z500 anomaly, spanning a 10^6 km^2 region, must occur in the same region as a reversal of the meridional absolute z500 gradient. Anomalies must be greater than a given threshold calculated using data from all longitudes and latitudes 30-90°N (data normalized by latitude); we use a threshold of 1 standard deviation [78]. In the original method the standard deviation is calculated for a 3-month period centred around the given month; to implement this for the forecasts using a methodology that could be operationalised (i.e., not relying on information from the future), we calculate the standard deviation based on all June values from ensemble members with June initializations across all available years. As the number of ensemble members varies between forecast (2021) and reforecast (2010-2020) years, standard deviations are calculated separately for each year and then averaged. The persistence requirement is considered to be satisfied if the events last for at least 5 days.

For comparison to ERA5 data in Fig. 3, the location of the observed event (grey contours) is determined by temperature anomalies greater than the 90th percentile and 5°C, and areas where there is blocking for at least 5 of the 7 days (25 June to 1 July inclusive).

Climate change context

Analysis of the change in mean and daily maximum temperatures was conducted using the Berkeley Earth temperature anomaly dataset [81]. We calculated a latitude-weighted mean of JJA monthly mean average, and monthly mean daily maximum land temperatures over the region 45N–52°N, 119W–123°W, as highlighted in Fig. 1a; results are relatively insensitive to changes to this region definition. We analyse data over the period 1875-2020, the time period for which there was a valid value for every gridbox over the selected region, whilst excluding the 2021 heatwave event. We calculate linear fits to approximate the change in annual mean temperatures, finding a value of 0.10°C/decade (p-value 0.4E-9) for annual mean temperatures, 0.07°C/decade (p-value 0.3E-5) for June-July-August (JJA) mean temperatures, and 0.04°C/decade (p-value 0.1) for JJA monthly mean daily max temperatures. For the period 1950-2020, these values are 0.22°C/decade (p-value 0.5E-6), 0.18°C/decade (p-value 0.1E-3) and 0.14°C/decade (p-value 0.07) respectively. The higher values for the past 70 years are

likely influenced by the reduction in aerosol emissions over the region during this time [14]; however, such reductions are likely to continue in the coming decades, and so this may be a more accurate representation of near-future trends [15].

The PAMIP simulations analysed are described in detail in Smith et al. (2019)[19], and were designed to isolate the impacts of sea ice loss and sea surface temperature (SST) changes on atmospheric circulation. The experiments we analyse use fixed SSTs and sea-ice concentration (SIC) as boundary conditions for an atmosphere-only general circulation model. To isolate the impact of sea ice loss alone on atmospheric circulation patterns, we compare simulations with present day SSTs and pre-industrial Arctic SIC (pdSST-piSIC), present day SSTs and present day SIC (pdSST-pdSIC), and present day SSTs with future Arctic SIC (pdSST-futArcSIC). We further contrast the present day simulations (pdSST-pdSIC) with those with pre-industrial SSTs and SIC (piSST-piSIC) to understand if changes in SST may have increased the probability of amplified atmospheric waves.

There are many available metrics of atmospheric 'waviness'; to avoid results that may be highly sensitive to the metric selected, we choose two metrics that use different variables on different levels within the atmosphere. The first is the finite-amplitude local wave amplitude (LWA) [82,83]; we calculate the LWA using geopotential height at 500 *hPa* (z500), a formulation which has been shown to be strongly connected to persistent weather systems [84], with the anti-cyclonic LWA (a-LWA) associated with blocking [85]. We analyse differences within the PAMIP simulations in a-LWA. The second metric used is an algorithm to detect recurrent, or quasi-stationary, Rossby waves [86,87]; this metric, *R*, uses meridional wind speeds at 250 *hPa* (v250). When applied to ERA-5 reanalysis data [58] both *R* and *a-LWA* show a positive anomaly over the Pacific Northwest region during the heatwave event relative to the 1979-2020 climatology for June/July, demonstrating their suitability as metrics for this type of event.

We analyse results from two models from the PAMIP project, the IPSL-CM6A-LR and CanESM5. These models were chosen as the only models with both z500 and v250 at the required daily temporal resolution available on the Earth System Grid at the time of research for the simulations studied. These two models cover a wide range of the different model responses of the mid-latitude circulation to sea ice loss within the PAMIP model ensemble, with the CanESM5 showing a strong reduction in mid-latitude zonal winds, and the IPSL-CM6A-LR a similar, but much weaker response [20]. We note that imposing sea ice loss alone misses other aspects of the AA response to anthropogenic warming [21], and the response may be sensitive to how or where AA is imposed [88,89].

Human health impacts

Mortality rates during and after the heatwave, and deaths attributed to the heatwave were sourced from coroners reports for BC[25] , State or Country reports for WA [26] and OR [90], and local news reporting for AB [91] and ID [92]. Non-fatal hospital admission data were from hospitals reporting to the National Syndromic Surveillance Program.

The notice from WorksafeBC advising employers to consider workplace closures during the extreme heat event can be found here: https://www.worksafebc.com/en/about-us/news-

events/news-releases/2021/June/worksafebc-advising-employers-to-consider-workplace-closures-during-heat-wave, with local news sources reporting that businesses followed this advice [93].

Marine Life

Mussel mortality surveys were conducted on a representative intertidal boulder field at the Porteau Cove Marine Park, BC (49.5613°N, -123.2336°W) on 8 July, 2021. The odor of rotting marine life was still pronounced at this site even 10-12 days after the peak of the heatwave. Randomly placed 100 cm^2 quadrats (n = 20) were used to determine the number of live and dead mussels. The mean mortality across quadrats was 73.6 +/- 6.2% (mean +/- s.e.), with an average of 10.0 +/- 1.8 dead mussels per 100 cm^2. The mussel population at this site occurred primarily in a zone 12 meters wide (cross-shore), suggesting that roughly 1,200,000 mussels died within the ~100 m alongshore extent of this boulder field. Although mussel shells remain attached to the shore via byssus for many weeks after death, we cannot rule out that our surveys slightly underestimated mortality due to shell loss (there was some evidence for this in some quadrats), or overestimated it by including previously dead animals (although the percentage of standing dead mussels is typically low).

Estimates of barnacle deaths were obtained from random quadrat sampling (n=25) of barnacles (*Balanus glandula*) at a gently sloping cobble and boulder shore (1001 Steps Park, 49.0306, -122.8752). Unlike mussels, which gape very soon after death (see Fig. 4c), barnacles can retain their opercular plates for several weeks after they have died, making mortality more difficult to discern visually. The barnacle mortality surveys reported here were conducted on 25 July, 2021, which allowed sufficient time for opercular plates of recently-deceased barnacles to wash away. Sampling revealed 80.6 +/- 5.7% mortality (mean +/- s.e.), which far exceeds the pre-heatwave background frequency of standing dead (7.9 +/- 1.2%). The number of excess dead barnacles per 100 cm^2 quadrat was 55.1 +/- 9.0. Scaling up to the entire barnacle zone at this site (18 m wide in the cross-shore direction) suggests this heatwave killed roughly 10 million barnacles along a single 100-m stretch of cobble shoreline. Qualitative (Raymond et al., in revision) and quantitative (Harley et al., unpublished data) surveys of barnacle and mussel mortality at other sites in BC and WA suggest that these high rates of mortality were experienced throughout much of Puget Sound and the Strait of Georgia, with lower but still noticeable mortality further north along the BC Central Coast.

Intertidal temperatures during the peak of the heatwave (the afternoon of 28 June 2021 in the vicinity of Vancouver, BC) were recorded with a FLIR E40 camera (Fig. 4a,b). The mortality of various species was documented opportunistically via additional photographs. The images in Fig. 4 were taken at the following locations and dates: (c) Lighthouse Park, West Vancouver, BC, 28 June 2021; (d,g,h) 1001 Steps Park, Surrey, BC, 11 July 2021; (e) Elliot Beach Park, Ladysmith, BC, 10 July 2021; (f) Stanley Park, Vancouver, BC, 12 July 2021; and (i) Selma Park, BC, 16 July 2021.

Wildfires

The Fire Weather Index System (FWI), combines components accounting for the effects of both fuel moisture and weather conditions on fire behavior [94]. The system iteratively tracks the local weather's effects on the forest vegetation moisture content, combining this with wind-affected fire spread rates to yield a dimensionless index value ranging on average from 0 to 30, where higher values represent the potential of extreme fire behavior.

The FWI values shown in Fig. 5 are derived and iteratively tracked using output from a numerical weather prediction (NWP) model. The NWP model used is the Weather Research, and Forecasting (WRFv4) Version 4.1.2 model initialized with the North American Mesoscale (NAM) model with two way nested domains of 36, 12, and 4 km [95]. All FWI parameters are solved within the 12km and 4km domains with output from the 4 km domain shown in Fig. 5. Further details of the WRF configuration and derived FWI values can be found here:
NWP Derived FWI: https://cerodell.github.io/fwf-docs/build/html/index.html
WRF configuration: http://weather.eos.ubc.ca/wxfcst/html-etc/model-metadata/wan00cg-01.html

Observed FWI data for Lytton, BC on 30 June was obtained from Natural Resources Canada's (NRCan) Canadian Wildfire Information System (CWFIS) FWI datamart (https://cwfis.cfs.nrcan.gc.ca/downloads/fwi_obs/) under Canada's Open Government Licence (https://open.canada.ca/en/open-government-licence-canada).

Smoke concentrations in Fig. 5 are outputs of ground-level smoke concentrations of particulate matter PM2.5 estimated from the BlueSky smoke forecasting system [96]. The BlueSky model was developed by the United States Forest Service (USFS) AirFire Research Group using inputs of fire information from satellite observations and meteorology to estimate fire emissions, initial smoke-plume rise, and subsequent 3-D smoke dispersion. The University of British Columbia (UBC) Weather Forecast and Research Team (WFRT) runs a version of the BlueSky model operationally (firesmoke.ca) during the wildfire season using satellite hotspot information from the smartfire algorithm and meteorology from the WRFv4 model mentioned above [97]. Hotspots are satellite image pixels with high infrared intensity, indicating a heat source and thus used as a proxy for wildfires.

Mid-tropospheric moisture is known to help produce thermodynamic conditions conducive for pyrocumulonimbus flammagenitus (CbFg) clouds to form over the burning wildfires [36,37,98,99]. These CbFg clouds can produce large amounts of lightning, providing ignition for more fires. Combustion of the forest vegetation produces smoke particles and releases additional water vapor into strong thermal updrafts above wildfires [36,100].

Data on wildfires were obtained from reports published online by the BC Wildfire Service (https://www2.gov.bc.ca/gov/content/safety/wildfire-status/about-bcws) and the Canadian Interagency Forest Fire Centre (https://www.ciffc.ca/). In particular, reports were accessed on the Sparks Lake fire [101] and the McKay Creek fire [102]. Data was also obtained from the CIFFC situational reports, in particular the report from July 11th [103], and those from July 1st, 2nd and 3rd [104–106].

Agriculture

The Normalized Difference Vegetation Index (NDVI) is often used to estimate crop yields [107] and is publicly available from Statistics Canada's Crop Condition Assessment Program (https://www35.statcan.gc.ca/CCAP/en/index). The NDVI is calculated during the growing season from 1,000 *m* resolution digital data from the National Oceanographic and Atmospheric Administration (NOAA) series of satellites and the 250 *m* MODIS digital data to monitor the changing vegetation conditions on a 7-day cycle over the agricultural region of Canada. We download these data for regions designated as "cropland" by the Crop Condition Assessment Program (CCAP), and spatially average over British Columbia.

Yield estimates were obtained from data made available by Statistics Canada. Provincial crop yields were obtained from Table 32-10-0359-01 "Estimated areas, yield, production, average farm price and total farm value of principal field crops, in metric and imperial units", https://doi.org/10.25318/3210035901-eng; regional crop yields from Table 32-10-0002-01 "Estimated areas, yield and production of principal field crops by Small Area Data Regions, in metric and imperial units", https://doi.org/10.25318/3210000201-eng; provincial fruit yields from Table 32-10-0364-01 Area, production and farm gate value of marketed fruits https://doi.org/10.25318/3210036401-eng; and provincial vegetable yields from Table 32-10-0365-01 Area, production and farm gate value of marketed vegetables, https://doi.org/10.25318/3210036501-eng.

Cryosphere and streamflow

Streamflow data were extracted from the Environment and Climate Change Canada Real-time Hydrometric data web site [108]. Snow water equivalent data were taken from the ERA5-Land hourly dataset[69]. Glacier area and location data are from the Randolph Glacier Inventory V6.0 [109], whilst basin areas and outlines are from the Water Survey of Canada [110]. Basin glacier coverage is calculated as the summed area of all glaciers[109] within a basin [110] divided by the basin area [108]. Code to reproduce the analyses and figures is available on GitHub (https://github.com/andersonsam/pacific_northwest_heatwave).

Record streamflow values were identified using the Hydrometric data from Environment Canada (https://wateroffice.ec.gc.ca/mainmenu/real_time_data_index_e.html). Examples of all-time record flows during this extreme heatwave are shown in Supplementary Fig. S3a-c, with figures obtained from the following links:

https://wateroffice.ec.gc.ca/report/real_time_e.html?stn=08KA005&mode=Graph&startDate=2021-03-01&endDate=2021-11-01&prm1=47&y1Max=&y1Min=&max1=1&upper1=1&lower1=1&prm2=47&y2Max=&y2Min=

https://wateroffice.ec.gc.ca/report/real_time_e.html?stn=08ME028&mode=Graph&startDate=2021-03-01&endDate=2021-11-01&prm1=47&y1Max=&y1Min=&max1=1&upper1=1&lower1=1&prm2=47&y2Max=&y2Min=

https://wateroffice.ec.gc.ca/report/real_time_e.html?stn=05DA009&mode=Graph&startDate=2021-03-01&endDate=2021-11-01&prm1=47&y1Max=&y1Min=&max1=1&upper1=1&lower1=1&prm2=47&y2Max=&y2Min=

Figure S3d shows daily streamflow records broken for consecutive days on the Lillooet River near Pemberton, where an evacuation order was issued, although the all-time record was not broken.
https://wateroffice.ec.gc.ca/report/real_time_e.html?stn=08MG005&mode=Graph&startDate=2021-03-01&endDate=2021-11-01&prm1=47&y1Max=&y1Min=&max1=1&upper1=1&lower1=1&prm2=47&y2Max=&y2Min=

During the heatwave event flood watches and warnings along with high streamflow advisories were issued by the BC River Forecast Centre (http://bcrfc.env.gov.bc.ca/warnings/index.htm) and an evacuation order was issued by the Squamish-Lillooet Regional District. Links to the notices can be obtained from the Emergency Info BC twitter account (@EmergencyInfoBC). Below we list links to the Evacuation order, as well as flood watches and flood warnings.

Squamish-Lillooet Regional District (2021). EVACUATION ALERT Issued for SLRD Electoral Area C - Pemberton Valley
https://www.slrd.bc.ca/sites/default/files/pictures/EOC/Evacuation%20ALERT%20%20-%20Electoral%20Area%20C%20-%20Pemberton%20Valley%20Flooding%20-%2026%20Jun%2021_0.pdf
Squamish-Lillooet Regional District (2021). EVACUATION ORDER Issued for SLRD Electoral Area C - Pemberton Valley
https://www.slrd.bc.ca/sites/default/files/pdfs/notices/Evacuation%20Order%20RESCIND%20-%20Electoral%20Area%20C%20-%20Pemberton%20Valley%20Flooding_June29_2021.pdf

Squamish-Lillooet Regional District (2021). Evacuation order rescind for Electoral Area C - Pemberton Valley
https://www.slrd.bc.ca/sites/default/files/pdfs/notices/Evacuation%20Order%20RESCIND%20-%20Electoral%20Area%20C%20-%20Pemberton%20Valley%20Flooding_June29_2021.pdf

Flood Watches (FWT) and Flood Warnings (FWN):
http://bcrfc.env.gov.bc.ca/warnings/advisories/FWT_2021_0630_1130CentralCoastSouthCoast_upg.pdf
http://bcrfc.env.gov.bc.ca/warnings/advisories/FWT_2021_0627_1315Chilcotin_upg.pdf
http://bcrfc.env.gov.bc.ca/warnings/advisories/FWN_2021_0630_0930_Chilcotin_upg.pdf
http://bcrfc.env.gov.bc.ca/warnings/advisories/FWT_2021_0626_1000_Lillooet_iss.pdf
http://bcrfc.env.gov.bc.ca/warnings/advisories/FWT_2021_0630_1330_Morice_upg.pdf
http://bcrfc.env.gov.bc.ca/warnings/advisories/FWT_2021_0628_730_UpperColumbia_upg.pdf
http://bcrfc.env.gov.bc.ca/warnings/advisories/FWT_2021_0627_1200UpperFraser_iss.pdf
http://bcrfc.env.gov.bc.ca/warnings/advisories/FWN_2021_06_29_1300UpperFraser_iss.pdf

Landslides

Post-wildfire debris flows were mapped from field observations and satellite imagery (Sentinel imagery dates 3 August, 2021; 28 August, 2021; 6 March, 2022) (Supplementary Fig. S5). Vegetation burn severity data produced by BC Ministry of Forests, Lands, Natural Resource Operations and Rural Development [111] using Normalized Burn Ratio (dNBR) and classified according to the United States Forest Service Burned Area Reflectance Classification (BARC) system [112]. Soil burn severity was also evaluated in the field to verify the classification of low, moderate, and high severity provided by the remotely-sense burn severity data. Field evaluation of burn severity was classified based on the apparent degree of mortality of the vegetative canopy and understory, depth of combusted organic matter in the soil and presence of water repellency. Shallow (<25 cm) test pits were hand dug to identify the percentage of ground cover burned, ash color and depth, changes to soil structure, depth to unburned roots, and soil water repellency. The test pits were accompanied by observations of the forest type and percentage of tree canopy burned. Soil burn severity corresponded to remotely sensed vegetation burn severity.

Methods-only references

58. Hersbach, H. *et al.* The ERA5 global reanalysis. *Quart. J. Roy. Meteor. Soc.* **146**, 1999–2049 (2020).
59. Angélil, O. *et al.* Comparing regional precipitation and temperature extremes in climate model and reanalysis products. *Weather Clim Extrem* **13**, 35–43 (2016).
60. Hersbach, H. *et al.* ERA5 hourly data on single levels from 1979 to present. *Copernicus Climate Change Service (C3S) Climate Data Store (CDS). (Accessed on 2022-01-27)* (2018) doi:10.24381/cds.adbb2d47.
61. Bell, B. *et al.* ERA5 hourly data on single levels from 1950 to 1978 (preliminary version). *Copernicus Climate Change Service (C3S) Climate Data Store (CDS). (Accessed on 2022-01-27)* (2020).
62. Donat, M. G. *et al.* Global Land-Based Datasets for Monitoring Climatic Extremes. *Bull. Am. Meteorol. Soc.* **94**, 997–1006 (2013).
63. Environment and Climate Change Canada. Technical documentation: Daily Climate Records (LTCE). https://www.canada.ca/en/environment-climate-change/services/climate-change/canadian-centre-climate-services/display-download/technical-documentation-daily-climate-records.html (2022).
64. Wei, M., Toth, Z., Wobus, R. & Zhu, Y. Initial perturbations based on the ensemble transform (ET) technique in the NCEP global operational forecast system. *Tellus Ser. A Dyn. Meteorol. Oceanogr.* **60**, 62–79 (2008).
65. Charron, M. *et al.* Toward Random Sampling of Model Error in the Canadian Ensemble Prediction System. *Mon. Weather Rev.* **138**, 1877–1901 (2010).
66. NCEP Central Operations. NCO IDSB - upcoming changes.
67. Bourdin, D. R., Nipen, T. N. & Stull, R. B. Reliable probabilistic forecasts from an ensemble reservoir inflow forecasting system. *Water Resour. Res.* **50**, 3108–3130 (2014).
68. Rex, D. F. Blocking Action in the Middle Troposphere and its Effect upon Regional Climate - Part I. *Tell'Us* **2**, 196–211 (1950).
69. Muñoz-Sabater, J. *et al.* ERA5-Land: a state-of-the-art global reanalysis dataset for land applications. *Earth Syst. Sci. Data* **13**, 4349–4383 (2021).
70. Vitart, F. *et al.* The Subseasonal to Seasonal (S2S) Prediction Project Database. *Bull. Am.*

Meteorol. Soc. **98**, 163–173 (2017).
71. Dai, G., Mu, M., Li, C., Han, Z. & Wang, L. Evaluation of the forecast performance for extreme cold events in east Asia with subseasonal-to-seasonal data sets from ECMWF. *J. Geophys. Res.* **126**, (2021).
72. Li, W. *et al.* Evaluation and Bias Correction of S2S Precipitation for Hydrological Extremes. *J. Hydrometeorol.* **20**, 1887–1906 (2019).
73. Xie, J., Yu, J., Chen, H. & Hsu, P.-C. Sources of Subseasonal Prediction Skill for Heatwaves over the Yangtze River Basin Revealed from Three S2S Models. *Adv. Atmos. Sci.* **37**, 1435–1450 (2020).
74. Leach, N. J., Weisheimer, A., Allen, M. R. & Palmer, T. Forecast-based attribution of a winter heatwave within the limit of predictability. *Proc. Natl. Acad. Sci. U. S. A.* **118**, (2021).
75. Zhu, H., Chen, H., Zhou, Y. & Dong, X. Evaluation of the subseasonal forecast skill of surface soil moisture in the S2S database. *Atmospheric and Oceanic Science Letters* **12**, 467–474 (2019).
76. Murphy, A. H. Probabilities, Odds, and Forecasts of Rare Events. *Weather Forecast.* **6**, 302–307 (1991).
77. Owens, R. G. & Hewson, T. *ECMWF Forecast User Guide*. https://confluence.ecmwf.int/display/FUG/Forecast+User+Guide (2018) doi:10.21957/m1cs7h.
78. Chan, P.-W., Hassanzadeh, P. & Kuang, Z. Evaluating indices of blocking anticyclones in terms of their linear relations with surface hot extremes. *Geophys. Res. Lett.* **46**, 4904–4912 (2019).
79. Dunn-Sigouin, E., Son, S.-W. & Lin, H. Evaluation of Northern Hemisphere Blocking Climatology in the Global Environment Multiscale Model. *Mon. Weather Rev.* **141**, 707–727 (2012).
80. Dunn-Sigouin, E. & Son, S.-W. Northern Hemisphere blocking frequency and duration in the CMIP5 models. *J. Geophys. Res. D: Atmos.* **118**, 1179–1188 (2013).
81. Rohde, R. A. & Hausfather, Z. The Berkeley Earth land/ocean temperature record. *Earth Syst. Sci. Data* **12**, 3469–3479 (2020).
82. Chen, G., Lu, J., Burrows, D. A. & Leung, L. R. Local finite-amplitude wave activity as an objective diagnostic of midlatitude extreme weather. *Geophys. Res. Lett.* **42**, 10,952–10,960 (2015).
83. Huang, C. S. Y. & Nakamura, N. Local Finite-Amplitude Wave Activity as a Diagnostic of Anomalous Weather Events. *J. Atmos. Sci.* **73**, 211–229 (2016).
84. Nakamura, N. & Huang, C. S. Y. Atmospheric blocking as a traffic jam in the jet stream. *Science* **361**, 42–47 (2018).
85. Martineau, P., Chen, G. & Burrows, D. A. Wave Events: Climatology, Trends, and Relationship to Northern Hemisphere Winter Blocking and Weather Extremes. *J. Clim.* **30**, 5675–5697 (2017).
86. Röthlisberger, M., Martius, O. & Wernli, H. An algorithm for identifying the initiation of synoptic-scale Rossby waves on potential vorticity waveguides: Initiation of Rossby Waves on PV Waveguides. *Q.J.R. Meteorol. Soc.* **142**, 889–900 (2016).
87. Röthlisberger, M., Pfahl, S. & Martius, O. Regional-scale jet waviness modulates the occurrence of midlatitude weather extremes. *Geophys. Res. Lett.* **43**, 2016GL070944 (2016).
88. Cvijanovic, I. *et al.* Future loss of Arctic sea-ice cover could drive a substantial decrease in California's rainfall. *Nat. Commun.* **8**, 1947 (2017).
89. Levine, X. J., Cvijanovic, I., Ortega, P., Donat, M. G. & Tourigny, E. Atmospheric feedback explains disparate climate response to regional Arctic sea-ice loss. *npj Climate and Atmospheric Science* **4**, 1–8 (2021).
90. Multnomah County. *Preliminary Review on Excessive Heat Deaths*. https://multco-web7-

psh-files-usw2.s3-us-west-2.amazonaws.com/s3fs-public/preliminary_review-heat_deaths-07-14-21_2.pdf (2021).
91. Johnson, L. Alberta saw spike in reported deaths during heatwave, causes still under investigation. *Edmonton Journal* https://edmontonjournal.com/news/local-news/alberta-saw-spike-in-reported-deaths-during-heatwave-causes-still-under-investigation (2021).
92. Schwedelson, P. Treasure Valley has a first death caused by heat wave. *Idaho Press* (2021).
93. Judd, A. B.C. businesses close their doors due to extreme heat. *Global News* https://globalnews.ca/news/7986877/bc-businesses-closing-monday-extreme-heat/ (2021).
94. Van Wagner, C. E. *Development and structure of the Canadian Forest Fire Weather Index System*. (Canada Communication Group Publ, 1987).
95. Skamarock, W. C. *et al. A Description of the Advanced Research WRF Model Version 4.1*. http://dx.doi.org/10.5065/1dfh-6p97 (2019) doi:10.5065/1dfh-6p97.
96. Larkin, N. K. *et al.* The BlueSky smoke modeling framework. *Int. J. Wildland Fire* **18**, 906 (2009).
97. Raffuse, S. M. *et al. SMARTFIRE Algorithm Description*. 9 https://firesmoke.ca/smartfire/pdfs/SMARTFIRE_Algorithm_Description_Final.pdf (2009).
98. Goens, D. W. & Andrews, P. L. *Weather and fire behavior factors related to the 1990 Dude Fire near Payson, AZ*. (Goens, David W and Andrews, Patricia L, 1998).
99. Trentmann, J. *et al.* Modeling of biomass smoke injection into the lower stratosphere by a large forest fire (Part I): reference simulation. *Atmos. Chem. Phys.* **6**, 5247–5260 (2006).
100. Warner, J. & Twomey, S. The Production of Cloud Nuclei by Cane Fires and the Effect on Cloud Droplet Concentration. *Journal of Atmospheric Sciences* **24**, 704–706 (1967).
101. BC Wildfire Service. Wildfires of Note: Sparks Lake (K21001). http://bcfireinfo.for.gov.bc.ca/hprScripts/WildfireNews/OneFire.asp?ID=811 (2021).
102. BC Wildfire Service. Wildfires of Note - Mckay Creek (K71030). https://bcfireinfo.for.gov.bc.ca/hprScripts/WildfireNews/OneFire.asp?ID=812 (2021).
103. Canadian Interagency Forest Fire Centre Inc. *National Fire Situation Report - July 11th*. https://ciffc.net/en/ciffc/sitrep/2021-07-11 (2021).
104. Canadian Interagency Forest Fire Centre Inc. *National Fire Situation Report - July 1st*. https://ciffc.net/en/ciffc/sitrep/2021-07-01 (2021).
105. Canadian Interagency Forest Fire Centre Inc. *National Fire Situation Report - July 2nd*. https://ciffc.net/en/ciffc/sitrep/2021-07-02 (2021).
106. Canadian Interagency Forest Fire Centre Inc. *National Fire Situation Report - July 3rd*. https://ciffc.net/en/ciffc/sitrep/2021-07-03 (2021).
107. Roznik, M., Boyd, M. & Porth, L. Improving crop yield estimation by applying higher resolution satellite NDVI imagery and high-resolution cropland masks. *Remote Sensing Applications: Society and Environment* **25**, 100693 (2022).
108. Water Survey of Canada. Historical Hydrometric Data (HYDAT). https://wateroffice.ec.gc.ca/mainmenu/historical_data_index_e.html.
109. RGI Consortium. Randolph Glacier Inventory – A Dataset of Global Glacier Outlines: Version 6.0. *Technical Report, Global Land Ice Measurements from Space, Colorado, USA. Digital Media.* (2017) doi:10.7265/N5-RGI-60.
110. Environment and Climate Change Canada. National hydrometric network basin polygons. https://open.canada.ca/data/en/dataset/0c121878-ac23-46f5-95df-eb9960753375 (2016).
111. BC Ministry of Forests, Lands, Natural Resource Operations and Rural Development (n.d.). 2021 Burn Severity Mapping. *Accessed on November 1, 2022* (2021).
112. Parsons, A., Robichaud, P. R., Lewis, S. A., Napper, C. & Clark, J. T. Field Guide for Mapping Post-Fire Soil Burn Severity. *United States Department of Agriculture, Forest Service* **General Technical Report RMRS-GTR-243**, (2010).

Supplementary Files

This is a list of supplementary files associated with this preprint. Click to download.

- SupplementaryInfoTheunprecedentedPacificNorthwestHeatwaveofJune2021.pdf